Phys Chem Minerals (1994) 21:117–132

PHYSICS AND CHEMISTRY OF MINERALS

A Crystallographic and Mössbauer Spectroscopy Study of $Fe_3^{2+}Al_2Si_3O_{12}-Fe_3^{2+}Fe_2^{3+}Si_3O_{12}$, (Almandine-"Skiagite") and $Ca_3Fe_2^{3+}Si_3O_{12}-Fe_3^{2+}Fe_2^{3+}Si_3O_{12}$ (Andradite-"Skiagite") Garnet Solid Solutions

Alan B. Woodland, Charles R. Ross II*

Bayerisches Geoinstitut, Universität Bayreuth, D-95440 Bayreuth, Germany

Received August 30, 1993 / Revised, accepted Februrary 12, 1994

Abstract. The crystal chemistry of garnet solid solutions on the $Fe_3^{2+}Al_2Si_3O_{12}-Fe_3^{2+}Fe_2^{3+}Si_3O_{12}$ (almandine-"skiagite") and $Ca_3Fe_2^{3+}Si_3O_{12}-Fe_3^{2+}Fe_2^{3+}Si_3O_{12}$ (andradite-"skiagite") joins have been investigated by single-crystal X-ray structure refinements and Mössbauer spectroscopy. Together, these two solid solution series encompass the complete range in $Fe^{3+}/\Sigma Fe$ from 0.0 to 1.0. All garnets are isotropic and were refined in the $Ia\bar{3}d$ space group.

Small excess volumes of mixing are observed in andradite-"skiagite" solid solutions ($W_v = 1.0 \pm 0.2$ cm^3 mol^{-1}) and along the almandine-"skiagite" join ($W_v = -0.77 \pm 0.17$ cm^3 mol^{-1}). The octahedral (Al, Fe^{3+})$-$O bond lengths show a much greater variation across the almandine-skiagite join compared to the andradite-skiagite garnets. The dodecahedral (X)$-$O bond lengths show the opposite behaviour. In andradite-"skiagite" solid solutions, the octahedral site passes from being flattened to elongated parallel to the $\bar{3}$ axis of symmetry with increasing "skiagite" content. A perfect octahedron occurs in a composition of $\approx$35 mol% "skiagite". The occupancy of the neighboring dodecahedral sites has the greatest effect on octahedral distortion and vice versa.

The Mössbauer hyperfine parameters of Fe^{2+} remain constant in both solid solutions. The hyperfine parameters of Fe^{3+} (at room temperature: centre shift = 0.32–0.40 mm/sec, quadrupole splitting (QS) $\approx$ 0.21–0.55 mm/sec) indicate that all Fe^{3+} is in octahedral coordination. The Fe^{3+} parameters are nearly constant in almandine-"skiagite" solid solutions, but vary significantly across the andradite-"skiagite" join. The structural unit that contributes to the electric field gradient of the octahedral site is different from that of the coordinating oxygen polyhedron, probably involving the neighboring dodecahedral sites.

$Fe^{3+}/\Sigma Fe$ area ratios derived from the Mössbauer spectra systematically overestimate Fe^{3+} contents in both solid solutions series. This is attributable to different recoil-free fractions for Fe on the octahedral and dodecahedral sites. A correction has been derived that yields more accurate $Fe^{3+}/\Sigma Fe$ ratios from room temperature and 80 K Mössbauer spectra.

Introduction

Silicate garnets are common in many geologic environments. As a result, garnet-bearing assemblages are often used to estimate conditions present in the Earth's crust and mantle. Making accurate estimates of geologic conditions from such assemblages requires a detailed knowledge of the physical and chemical properties of garnets. Understanding the effects of cation substitution on crystal structure provides a microscopic basis for explaining observed non-ideal thermodynamic behaviour and can give important indications for likely non-ideality in garnets for which thermodynamic data is lacking.

Garnets are cubic (space group $Ia\bar{3}d$) with a general formula $\{X_3\}[Y_2](Z_3)O_{12}$, where $\{\}$, $[]$, and $()$ denote dodecahedral, octahedral, and tetrahedral sites respectively (notation after Geller 1967). Naturally occurring garnets are complex solid solutions involving extensive cation substitution on the dodecahedral and octahedral sites. Winchell (1933) subdivided the garnet group into two series based upon a distinct break in the observed compositions of natural garnets: 1) pyralspites, where Y = Al and X $\neq$ Ca; and 2) ugrandites, where X = Ca. An implication of this classification is that the substitution of the large Ca cation into the dodecahedral site has an important effect on the garnet structure.

Many X-ray crystal structure studies have been performed on a variety of garnets, often considering one particular composition. Novak and Gibbs (1971) refined the structure of eight natural garnets and a synthetic pyrope in order to study how cations of different size are accomondated in the garnet structure. They established a relationship between the oxygen positional parameters and the average radii of the dodecahedral and

* *Present address:* Department of Chemistry, 718 Hamilton Hall, University of Nebraska, Lincoln, Nebraska, 68588-0304, USA

octahedral cations. They also noted that the dodecahedral – octahedral shared edge was longer than the octahedral unshared edge in grossular ($Ca_3Al_2Si_3O_{12}$), of the ugrandite series, whereas the opposite was true in the pyralspite garnets. Recently, Armbruster et al. (1992) reported single-crystal refinements of several synthetic almandine – pyrope solid solutions. They concluded that there was no structural evidence to support large non-ideality across the join, in agreement with the $Mg-Fe^{2+}$ partitioning studies of O'Neill and Wood (1979) and Hackler and Wood (1989).

Mössbauer spectroscopy of Fe-bearing garnets provides crystal chemical information that is complimentary to X-ray diffraction data by revealing the site occupancy and valence state of Fe. Detail of the local electronic environment about the Fe atoms can also be assessed from the calculated hyperfine parameters. A number of Mössbauer spectroscopic studies of garnets have been reported in the literature, most concerning garnets with a narrow range of composition. The most extensive study is that by Amthauer et al. (1976) who analysed 15 natural garnets of different composition. They reported ranges in hyperfine parameters corresponding to dodecahedrally and tetrahedrally coordinated Fe^{2+} and octahedrally and tetrahedrally coordinated Fe^{3+} and related variations in hyperfine parameters to garnet composition. It is important to note that 10 of their 15 garnets contained both Fe^{2+} and Fe^{3+}.

The purpose of our study is to investigate the relative effects of octahedral and dodecahedral site substitutions on the structure and site environments of Fe-bearing garnets. We report results of single-crystal structure refinements and Mössbauer spectroscopy obtained from two binary garnet solid solutions: $Fe_3^{2+}Al_2Si_3O_{12}-Fe_3^{2+}Fe_2^{3+}Si_3O_{12}$, (almandine-skiagite) and $Ca_3Fe_2^{3+}Si_3O_{12}-Fe_3^{2+}Fe_2^{3+}Si_3O_{12}$ (andradite – skiagite). Although skiagite has been discredited as a proper mineral name, we retain the term here to refer to an end-member component that may occur in complex garnet solid solutions. For the almandine-skiagite garnets, $Al-Fe^{3+}$ mixing occurs on the octahedral sites, while in andradite-skiagite garnets Fe^{2+} substitutes for Ca on the dodecahedral sites. The partial occupancy of Ca and the presence of octahedral Fe^{3+} means that these solid solutions have compositions that are continuous between the pyralspite and ugrandite series of Winchell (1933). Their $Fe^{3+}/\Sigma Fe$ ranges from 0.0 in almandine to 0.4 in skiagite to 1.0 in andradite. The respective recoil-free fractions for Fe^{2+} and Fe^{3+} on the dodecahedral and octahedral sites can be evaluated because the simple chemical composition of the garnets permits the $Fe^{3+}/\Sigma Fe$ to be determined independently from the microprobe if perfect stoichiometry and charge balance are assumed.

Aside from the unit cell edge measurements for almandine-skiagite solid solutions given by Woodland and O'Neill (1993), no work has been reported on garnets containing the skiagite component. However, other garnet solid solutions have analogous cation substitutions. Dodecahedral $Ca-Fe^{2+}$ exchange occurs along the almandine-grossular binary and octahedral $Al-Fe^{3+}$ exchange occurs in andradite-grossular garnet solid solutions. A drawback to studying these two solid solutions is that the synthesis of true binary garnets requires that Fe is present in only one oxidation state, which is experimentally difficult to attain (e.g. Huckenholz et al. 1974; Geiger et al. 1987; Woodland and Wood 1989). Inspite of this potential problem, almandine-grossular garnets have been extensively studied in terms of their macroscopic thermodynamic properties (Cressey et al. 1978; Geiger et al. 1987; Koziol 1990) and their microscopic structural properties (Geiger et al. 1990). Unfortunately, no systematic structural study has been made across this binary join.

The andradite-grossular join has received less attention. Several detailed crystallographic studies have been carried out on natural birefringent (and therefore non-cubic) garnets with compositions close to the andradite-grossular join (Takeuchi et al. 1982; Allen and Buseck 1988; Kingma and Downs 1989; Soós et al. 1991). Several explanations for the deviation from cubic symmetry have been proposed including lattice strain, the presence of OH as a hydrogarnet component, and ordering of Fe^{3+} and Al on distinct octahedral sites. Aside from these apparently anomalous garnets, no detailed structural studies have been made. Phase equilibria and synthesis studies involving andradite-grossular solid solutions have been made by Holdaway (1972), Liou (1973), Perchuk and Aranovich (1979), and Huckenholz et al. (1974, 1981, 1982). Ideal mixing across the join is reported by Holdaway (1972) and Perchuk and Aranovich (1979), however, this was disputed by Engi and Wersin (1987), based upon data from Huckenholz et al. (1974, 1981). This is potentially important since the large Ca cation in andradite-grossular garnets expands the garnet structure relative to the pyralspite garnets and could make it easier to accommodate a larger octahedral cation.

Experimental Procedures

Synthesis

The garnets were synthesised in a piston-cylinder apparatus and a multi-anvil press at 1080° C or 1100° C at pressures between 1.7 and 9.7 GPa following the methods described in Woodland and O'Neill (1993). Starting materials were glasses or slags prepared by melting stoichiometric amounts of Fe_2O_3, SiO_2, and Al_2O_3 or decarbonated $CaCO_3$ (for almandine-bearing and andradite-bearing compositions respectively) at 1500° C or 1550° C. The correct $Fe^{3+}/\Sigma Fe$ ratio was achieved by controlling the fO_2 of the furnace atmosphere using $CO-CO_2$ or $Ar-O_2$ gas mixes and using $fO2$ values estimated from Figure 6902 in Roth et al. (1987, p. 454–546) and calculated from Kress and Carmichael (1988). Glasses of 90% and 80% andradite composition were produced in air at 1475° C and 1550° C respectively.

The garnet compositions and unit cell parameters are given in Table 1, along with the conditions of synthesis. The compositions were determined using a Cameca Camebax SX50 microprobe in wavelength dispersive mode using a 15 kV accelerating voltage and a 15 nA beam current. The standards were Fe_2O_3 for Fe, spinel for Al, andradite for Ca, and either andradite or orthoclase for Si. The raw counts were processed using the PAP correction procedure supplied by Cameca. Garnet compositions were calculated assuming ideal stoichiometry of 8 cations per formula unit and charge balance.

All garnets used in this study are isotropic under oils. The almandine-skiagite garnets are pinkish at low (alm 85) skiagite content and take on a dark red-brown colour at skiagite-rich compositions (alm 11). The andradite-skiagite garnets are light yellow-brown at andradite-rich (> and 70) compositions and become progressively darker and redder with increasing skiagite content.

X-ray Diffraction

Unit cell parameters were determined by powder X-ray diffraction from the average of at least 10 peaks above 60° 2θ using single-crystal Ge monochromated Co K_{α_1} radiation and NBS Si metal as an internal standard (STOE STADIP focussing diffractometer in transmission mode). For some samples Ge metal, calibrated against Si metal, was used as the internal standard to avoid peak overlap problems.

Candidate crystals for singe-crystal structure refinement were selected and mounted on an Enraf-Nonius CAD4 diffractometer using graphite-monochromated Mo K_α radiation ($K_{\alpha_1}=0.70930$, $K_{\alpha_2}=0.71359$). The crystal quality was evaluated through the examination of rotation photographs and the mapping of selected reflections in reciprocal space, until a satisfactory crystal was found. After determination and refinement of the orientation matrix, one-sixteenth of reciprocal space ($h, k \geq 0, 1 \geq k$) to $\sin\Theta/\lambda \approx 1.0$ ($\Theta = 45°$) was collected in $\omega - \Theta$ scan mode. Crystal alignment was checked after the collection of every 150 reflections, the intensity of standard reflections was checked every hour. After data collection, ψ-scan data were collected for the application of an empirical absorption correction.

The data were corrected for Lorenz and polarization effects, as well as for absorption. Symmetrically equivalent data were averaged, with a R_{merge} between 1.5% and 3.7% (Table 2). Structure factors were weighted using a modified Poisson weighting scheme. The data were examined for evidence of lowered space-group symmetry, but no systematic deviation from $Ia\bar{3}d$ was found. A total of 17 parameters were refined, i.e. the scale factor, the oxygen positional parameters, and anisotropic temperature factors (13 variables). Table 2 lists the final R factors and structural parameters and Table 3 lists the final anisotropic atomic displacement parameters. A listing of observed and final calculated structure factors may be obtained from the authors.

Mössbauer Spectroscopy

Transmission Mössbauer spectra were collected at 298 K and 80 K with a Mössbauer spectrometer operating in constant acceleration mode and a nominal 50 mCi ^{57}Co in a 6 μm Rh matrix. The velocity ramp was ±5 mm/sec. Mirror-image spectra were collected over 512 channels and calibrated with respect to 25 μm α−Fe metal at room temperature. Spectra obtained at a sample temperature of 80 K (source at 298 K) employed a variable temperature cold-finger cryostat that controls temperature to ±0.5 K. The samples were prepared so that the Fe concentration was between 2 and 5 mg/cm^2 to avoid saturation effects. Most samples were mounted on plastic foil while some samples were mixed with benzophenone and mounted in acrylic holders. The spectra were fit to Lorenzian line shapes with the peak areas and full widths at half maximum (FWHM) of each doublet constrained to be equal (see below). This was done using the PC−MOS software obtained from CMTE Elektronik, Auenstraße 15, D-85521 Riemerling, FRG. Some spectra were also fit using the Missfita program (see Luth et al. 1990) and were found to give the same hyperfine parameters and area ratios within the uncertainties of ±0.01 mm/sec and ±0.01 respectively.

Table 1. Synthesis conditions, composition, and unit cell edges for andradite-skiagite and almandine-skiagite garnet solid solutions

Sample	Temp (°C)	Pressure (GPa)	Duration (hr)	Comp X_{and}	Cell edge (Å)
andradite-skiagite solid solutions					
and23	1300	1.3	4	1.00	12.0690 (5)
aw63	1100	1.2	91	1.00	12.0596 (2)
aw39a	1080	2.8	72	0.94	12.0457 (15)
aw54a	1080	2.5	93	0.93	12.0375 (1)
aw54b	1080	2.5	93	0.92	12.0361 (7)
aw48	1100	1.7	116	0.88	12.0255 (8)
aw46	1000	1.6	24	0.83	12.0161 (7)
aw39b	1080	2.8	72	0.82	12.0045 (6)
aw40	1080	3.6	72	0.75	11.9807 (7)
aw41	1100	3.9	90	0.73	11.9803 (6)
aw52a	1100	4.1	97	0.72	11.9755 (1)
aw52b	1100	4.1	97	0.67	11.9565 (7)
aw52c	1100	4.1	97	0.66	11.9572 (5)
aw47*	1100	4.8	46	0.64	11.9503 (8)
u769	1100	5.4	12.5	0.60	11.9382 (3)
u769r	1100	5.4	12.5	0.59	11.9290 (9)
u659a	1100	6.0	12.5	0.53	11.9150 (7)
u659b*	1100	6.0	12.5	0.52	11.9150 (4)
u751a	1100	8.0	12.5	0.47	11.8911 (6)
u697	1100	7.0	12.5	0.45	11.8880 (5)
u654a	1100	7.0	12.5	0.37	11.8612 (6)
u684a	1100	7.5	12.5	0.36	11.8580(5)
u654b*	1100	7.0	12.5	0.36	11.8568 (7)
u751b	1100	8.0	12.5	0.36	11.8541 (7)
u684b	1100	8.0	12.5	0.36	11.8546 (4)
u714a	1100	8.5	12.5	0.26	11.8204 (6)
u610	1100	8.5	12	0.22	11.8025 (6)
u666*	1100	9.3	12.5	0.21	11.8002 (5)
u714b	1100	8.5	12.5	0.20	11.7923 (9)
u739*	1100	9.7	12.5	0.11	11.7663 (2)
u755	1100	9.0	12.5	0.11	11.7683 (7)

Sample	Temp (°C)	Pressure (GPa)	Duration (hr)	Comp X_{alm}	Cell edge (Å)
almandine-skiagite solid solutions					
alm1	1200	2.0	42	1.00	11.5285 (2)
alm6	1200	1.9	44	1.00	11.5285 (2)
aw18	1200	3.0	24	0.98	11.5299 (5)
aw14	1100	1.7	24	0.98	11.5312 (8)
aw45	1080	2.7	101	0.93	11.5405 (2)
aw25	1080	2.7	46	0.92	11.5400 (6)
aw26	1080	2.7	96	0.92	11.5390 (9)
aw30	1080	2.7	97	0.91	11.5408 (3)
aw37a*	1100	4.0	96	0.85	11.5546 (4)
aw37b	1100	4.0	96	0.79	11.5571 (5)
aw47	1100	4.8	46	0.70	11.5837 (7)
u458	1100	6.0	11	0.71	11.5777 (7)
u758	1100	6.5	12	0.61	11.6034 (7)
u541	1100	6.5	12	0.59	11.6061 (9)
u627	1100	7.0	12.5	0.50	11.6273 (3)
u765	1100	8.0	12.5	0.48	11.6283 (7)
u497	1100	9.0	12	0.21	11.6841 (7)
u524	1100	9.0	11	0.18	11.6903 (7)
u598*	1100	9.5	14	0.10	11.7076 (7)
u636	1100	10.0	12.5	0.01	11.7270 (6)
u702	1100	9.7	12.5	0.00	11.7272 (7)

* these samples were used in the single-crystal structure refinements aw47 = and36, u659b = and52, u684b = and64, u666 = and21, u739 = and11, aw37a = alm85, u598 = alm10

Unit Cell Edge and Molar Volumes

$Ca_3Fe_2^{3+}Si_3O_{12}-Fe_3^{2+}Fe_2^{3+}Si_3O_{12}$ Solid Solutions

The measured unit cell parameters are presented in Table 1 and Fig. 1. The unit cell parameter decreases almost linearly with increasing skiagite content. However, comparison with the linear fit shown in Fig. 1 reveals a slight asymmetry across the andradite-skiagite join. The unit cell parameters obtained from the andradite and skiagite end-members are $a_O = 12.0596(2)$ Å and $a_O = 11.7278(6)$ Å respectively. Our value for andradite is in excellent agreement with the values reported by Huckenholz and Yoder (1971), but somewhat smaller than the value of $a_O = 12.063(1)$ Å measured by Armbruster and Geiger (1993). A least squares refinement of our data (n = 34) gives $a_O = 12.0677(14) - 0.3359(23)X_{ski}$ with a $\chi_v^2 = 1.34$. A quadratic fit of $a_O = 12.0610(12) - 0.2957(55)X_{ski} - 0.0393(54)X_{ski}^2$ with a $\chi_v^2 = 0.53$ fits the andradite and skiagite end-member values better than the simpler linear fit, although the χ_v^2 value suggests that the data are overfit with the quadratic term.

One andradite sample not included in the above fitting had a somewhat larger unit cell edge of $a_O = 12.0690(5)$ Å. This andradite was crystallised from a glass at 1300° C and 1.4 GPa along with some PtO_2 in order to create a high $fO2$ and maintain all the Fe in the ferric state. Microprobe analysis revealed about 1 *wt* % Pt in this garnet, presumably residing on the octahedral site because of high crystal field stabilisation energies favouring this site. The presence of a small amount of Pt, with its relatively large ionic radius (0.8 Å for Pt^{2+}), explains the enlarged unit cell found in this particular garnet.

The molar volumes and excess volumes of mixing of the andradite-skiagite solid solutions can be derived directly from the unit cell parameters described above. A plot of excess volume against composition is shown in Fig. 2a, revealing small positive excess volumes of mixing. A symmetric fit yields $W_V = 1.0 \pm 0.2$ cm^3 mol^{-1} ($\chi_v^2 = 0.54$).

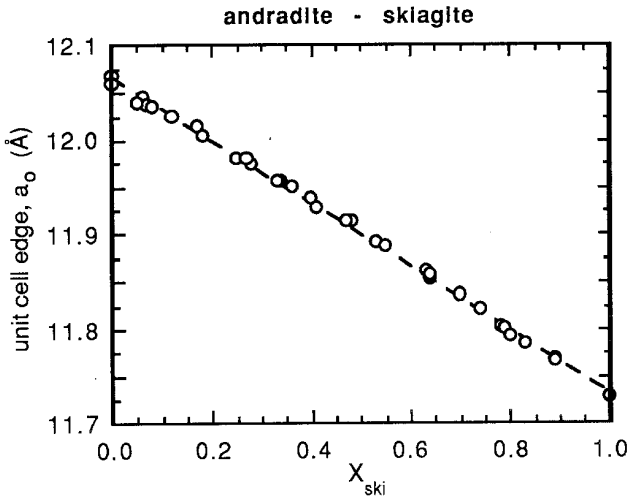

Fig. 1. Unit cell parameter, a_0, plotted as a function of skiagite content in andradite-skiagite solid solutions. Uncertainties are equal to or less than the size of the symbols

$Fe_3^{2+}Al_2Si_3O_{12}-Fe_3^{2+}Fe_2^{3+}Si_3O_{12}$ Solid Solutions

Unit cell parameters vary linearly across the almandine-skiagite join, as was reported in Woodland and O'Neill

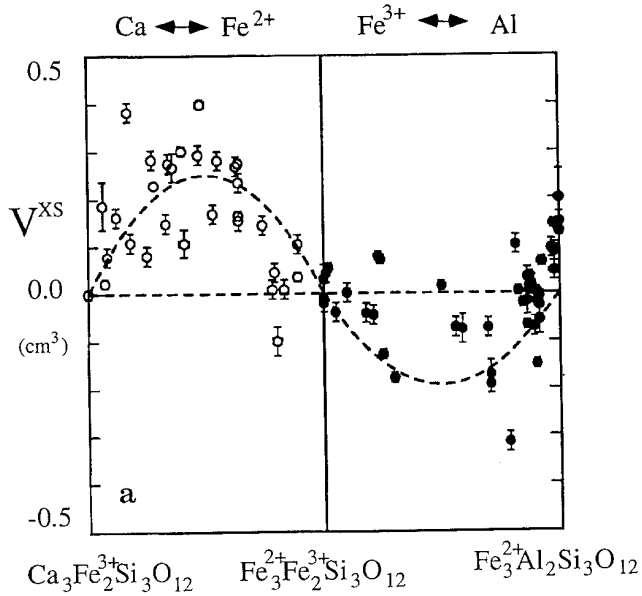

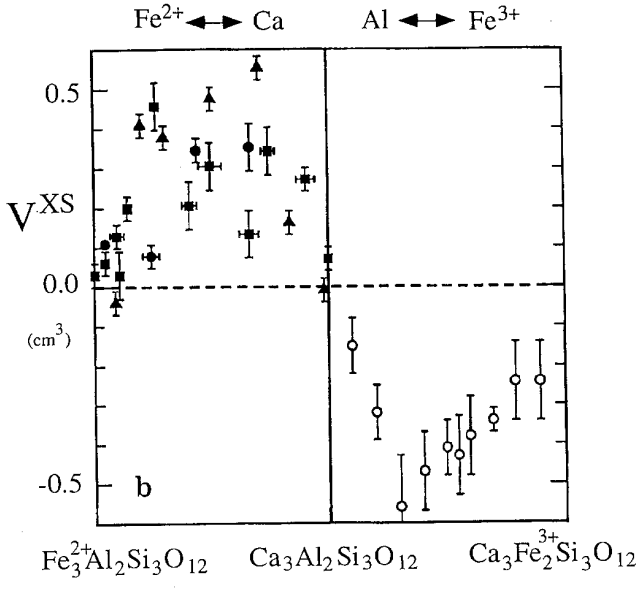

Fig. 2. Excess volumes of mixing in (**a**) andradite-skiagite and almandine-skiagite solid solutions (this study) and (**b**) almandine-grossular and andradite-grossular solid solutions (data from: *triangles*, Cressey et al. 1978; *squares*, Geiger et al. 1987; *circles*, Koziol 1990; *open circles*, Huckenholz et al. 1974). In **a**, the *dashed lines* are our least squares fits to the data. Where the error bars are not visible, the errors are less than the size of the symbols, except for the data of Cressey et al. (1978) and Huckenholz et al. (1974)

(1993). The unit cell parameters for the subset of garnets analysed by Mössbauer spectroscopy in this study are provided in Table 1. Small negative excess volumes of mixing are indicated for the almandine-skiagite solid solutions (Fig. 2a). Least squares refinement of the data yields $W_V = -0.77 \pm 0.17$ cm^3 mol^{-1} ($\chi^2_v = 1.72$). The apparent minor asymmetry towards the almandine end of the join was not statistically significant, presumably due to the scatter in the data. This behaviour contrasts with the positive deviations observed for the andradite-skiagite solid solutions.

Comparison with other Garnet Solid Solutions

Excess volumes of mixing for grossular-bearing solid solutions with the analogous cation substitutions are shown in Fig. 2b. Data for almandine-grossular garnets from Cressey et al. (1978), Geiger et al. (1987), and Koziol (1990) indicate small positive excess volumes of mixing, like that observed in our andradite-skiagite garnets. Likewise, the andradite-grossular solid solutions (from Huckenholz et al. 1974) show negative excess volumes of mixing, similar to that observed in our almandine-skiagite solid solutions. The magnitude of the negative deviations in the andradite-grossular solid solutions are not well constrained, however, since the reported compositions are only nominal compositions and the run products were too fine grained for electron microprobe analysis (H. Huckenholz, personal communication). An asymmetry towards the Al-bearing end-member is also apparent in the andradite-grossular solid solutions. It appears that substitution of Fe^{3+} for Al on the octahedral sites has the same effect on molar volume (slightly negative excess volumes) independent of the dodecahedral site occupancy. Likewise, similar positive excess volumes of mixing are observed when Ca substitutes for Fe^{2+} on the dodecahedral sites regardless of the octahedral site occupancy. Although small positive excess volumes are also observed in pyrope-grossular solid solutions (Ganguly et al. 1993), no generalised relationship involving Ca substitution holds since Koziol (1990) reports ideal volumes of mixing across the spessartine-grossular join.

Crystal Structure Analyses

Single-crystal X-ray structure refinements were obtained from 2 almandine-skiagite and 5 andradite-skiagite garnets. We can combine our results with those of Armbruster et al. (1992) and Armbruster and Geiger (1993) for the almandine and andradite end-members respectively. We were unable to obtain suitable single crystals of the skiagite end-member, although the and11 and alm10 samples place strong constraints on the structural parameters for skiagite. Predicted parameter values of skiagite from Novak and Gibbs (1971) are shown in the figures for comparison and are generally in good agreement with extrapolations from our data.

Comparison of the oxygen parameters in the almandine-skiagite samples indicate a shift of the oxygen atoms away from the octahedral sites with increasing skiagite content (Table 2). This is expected since the larger Fe^{3+} cation replaces Al on the octahedral sites across the join. In the andradite-skiagite solid solutions, there is a systematic movement of the oxygen atoms towards the dodecahedral site as Fe^{2+} substitutes for Ca. This behaviour is also not surprising since dodecahedrally coordinated Fe^{2+} is smaller than Ca (0.92 Å vs 1.12 Å, Shannon 1976).

Bond Lengths and Polyhedral Volumes

Variations in bond lengths and polyhedral volumes in the two garnet solid solution series depend on the site on which cation substitution occurs and the relative size of the substituting cation (Table 4). The polyhedral volumes show the same trends as the cation-oxygen bond lengths. In almandine-skiagite solid solutions, there is substantial elongation of the octahedral cation-oxygen (Y–O) bond lengths with increasing skiagite content, which is consistent with the substitution of the larger Fe^{3+} atom for Al on the octahedral sites (Fig. 3a). On the other hand, the two inequivalent dodecahedral bond lengths $(X-O)_1$, $(X-O)_2$ remain relatively constant (Fig. 3b). There is, however, a slight inequality between the relative elongation of $(X-O)_1$ and $(X-O)_2$ implying a change in the distortion of the dodecahedral site. Since 4 of 18 dodecahedral edges are shared with neighboring octahedral sites that are undergoing inflation and rotation, a change in figure of the dodecahedral sites would be expected.

In andradite-skiagite solid solutions, where Fe^{2+} substitutes for Ca on the dodecahedral sites, the $(X-O)_1$ and $(X-O)_2$ bond lengths undergo considerable shortening with increasing skiagite content (Fig. 3b). There

Table 2. *R* factors (%) and structural parameters from single crystal X-ray refinements

	R_m	R^a	R_{wb}	N_{obs}	x^0	y^0	z^0
alm85	3.7	1.9	2.8	113	0.0344 (2)	0.0500 (2)	0.6536 (2)
alm10	2.5	1.7	2.6	332	0.0352 (1)	0.0529 (1)	0.6568 (1)
and11	2.0	1.9	2.7	262	0.0357 (1)	0.0525 (1)	0.6571 (1)
and21	2.0	1.7	2.3	182	0.0362 (1)	0.0520 (1)	0.6571 (1)
and36	2.2	1.7	2.5	195	0.0364 (1)	0.0508 (1)	0.6568 (1)
and52	1.5	1.8	2.7	280	0.0370 (1)	0.0504 (1)	0.6564 (1)
and64	2.0	1.7	2.7	221	0.0378 (1)	0.0498 (1)	0.6561 (1)

[a] $R = \Sigma |F_{obs} - F_{calc}| / \Sigma |F_{obs}|$

[b] $R_w = \Sigma w (F_{obs} - F_{calc})^2 / \Sigma w F_{obs}^2]^{1/2}$, w is the weight

Table 3. Cation and Oxygen atomic displacement coefficients (U values $\times 10^4$)

	Cations						
	U_{11}^X	U_{22}^X	U_{23}^X	U_{11}^Y	U_{12}^Y	U_{11}^Z	U_{22}^Z
alm85	35(4)	84(2)	5(4)	39(3)	9(4)	22(7)	34(4)
alm10	53(1)	112(1)	13(1)	50(1)	1(1)	45(2)	54(1)
and11	53(1)	114(1)	14(1)	50(1)	0(1)	51(2)	51(1)
and21	54(2)	120(1)	11(2)	54(1)	1(2)	62(4)	53(2)
and36	52(2)	118(2)	21(3)	53(1)	−1(1)	74(4)	46(2)
and52	59(1)	125(1)	21(1)	62(5)	−2(1)	83(2)	55(1)
and64	58(2)	122(1)	28(2)	59(1)	−3(1)	80(3)	47(2)
	Oxygens						
	U_{11}^O	U_{22}^O	U_{33}^O	U_{12}^O	U_{13}^O	U_{23}^O	
alm85	63(8)	81(8)	34(8)	7(6)	−5(7)	0(8)	
alm10	74(2)	94(2)	69(2)	15(2)	−12(2)	0(2)	
and11	91(3)	94(3)	63(3)	18(3)	−20(3)	−9(3)	
and21	98(6)	95(5)	60(5)	11(5)	−12(5)	−8(5)	
and36	107(5)	86(5)	67(5)	18(5)	−13(5)	−4(5)	
and52	134(3)	92(3)	71(2)	19(3)	−16(2)	−2(2)	
and64	118(4)	78(4)	61(4)	16(4)	−17(4)	−1(4)	

The form of the anisotropic thermal vibration parameter for the garnet structure is: $\exp[-2\pi^2 a^{*2}\{h^2 U_{11}+k^2 U_{22}+l^2 U_{33}+2hkU_{12}+2hlU_{13}+2klU_{23}\}]$, where a is the reciprocal lattice constant. For the dodecahedral site, $\{X\}$, at (1/8, 0, 1/4), $U_{22}=U_{33}$, $U_{12}=U_{13}=0$; for the octahedral site, $[Y]$, at (0, 0, 0), $U_{11}=U_{22}=U_{33}$, $U_{12}=U_{13}=U_{23}$; and for the tetrahedral site, (Z), at (3/8, 0, 1/4), $U_{22}=U_{33}$, $U_{12}=U_{13}=U_{23}=0$

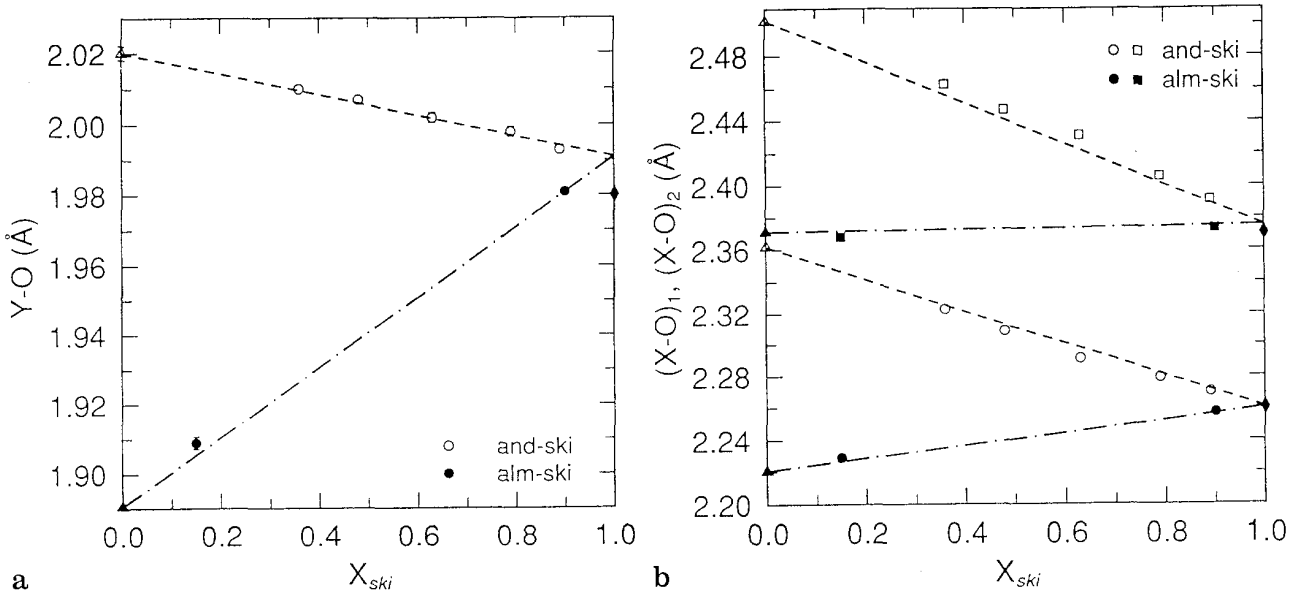

Fig. 3. Variation in **a** Y−O and **b** $(X-O)_1$ and $(X-O)_2$ bond lengths as a function of composition in andradite-skiagite and almandine-skiagite solid solutions. Data for the almandine (*closed triangle*) and andradite (*open triangle*) endmembers are from Armbruster et al. (1992) and Armbruster and Geiger (1993). The values for skiagite (*closed diamond*) are those predicted by Novak and Gibbs (1971)

is also a reduction in the Y−O bond lengths with increasing skiagite content (Fig. 3a). This is due to the fact that 6 of 12 octahedral edges are shared with neighboring dodecahedral sites so that when the dodecahedral site deflates, a concommitant change in the octahedral site is required. This change is manifested in a shortening of the Y−O bond lengths and a change in the degree and type of distortion of the octahedral site (see below).

The tetrahedral (Z−O) bond lengths and site volumes undergo only very minor changes of ≈0.005 Å in almandine-skiagite garnets and ≈0.01 Å in andradite-skiagite garnets (Table 4). A similar small variation in Z−O

Table 4. Interatomic distances (Å) and polyhedral volumes (Å^3)

	$(X-O)_1$ (×4)	$(X-O)_2$ (×4)	Y−O (×6)	Z−O (×4)	O−O[a] (Y, s)	O−O[a] (Y, u)	V_X (Å^3)	V_Y (Å^3)	V_Z (Å^3)
alm[b]	2.3712	2.2208	1.8904	1.6352	2.6422	2.7044	20.82	9.00	2.20
alm85	2.368	2.229	1.909	1.634	2.666	2.732	20.85	9.26	2.19
alm10	2.373	2.257	1.981	1.637	2.756	2.846	21.20	10.35	2.21
ski[c]	2.37	2.26	1.98	1.64	2.757	2.855	21.18	10.40	2.23
and11	2.391	2.270	1.993	1.638	2.781	2.857	21.63	10.55	2.21
and21	2.406	2.279	1.998	1.636	2.796	2.855	22.02	10.63	2.21
and36	2.431	2.291	2.002	1.640	2.811	2.853	22.54	10.70	2.22
and52	2.447	2.309	2.007	1.644	2.827	2.851	23.01	10.78	2.24
and64	2.463	2.323	2.010	1.643	2.842	2.841	23.44	10.82	2.24
an100[d]	2.502	2.362	2.020	1.648	2.881	2.832	24.56	10.98	2.27

[a] Y, s and Y, u refer to octahedral edges that are shared (with dodecahedra) and unshared respectively
[b] from Armbruster et al. (1992)
[c] predicted by Novak and Gibbs (1971)
[d] from Armbruster and Geiger (1993)

Table 5. Polyhedral distortion indicies

	QE'_Y[a]	AV_Y	QE'_Z	AV_Z	τ[b]	σ[c]	φ[c]	α[b]
alm[d]	53	1.936°	1291	53.04°	50.11°	53.80°	3.67°	26.75°
alm85	59	2.150°	1266	51.97°	50.16°	53.75°	3.38°	27.42°
alm10	100	3.647°	1334	54.79°	50.04°	53.44°	2.72°	29.58°
ski[e]	118	4.314°	1315	53.99°	50.07°	53.34°	2.56°	29.81°
and11	71	2.586°	1316	54.041°	50.07°	53.65°	2.82°	29.47°
and21	44	1.585°	1268	52.067°	50.16°	53.89°	2.91°	29.24°
and36	21	0.757°	1280	52.577°	50.14°	54.14°	3.22°	28.59°
and52	7	0.244°	1165	47.792°	50.39°	54.40°	3.16°	28.30°
and64	0	0.000°	1017	41.69°	50.64°	54.75°	3.19°	27.94°
and100[f]	29	1.023°	770	31.55°	51.16°	55.42°	3.19°	29.56°

[a] QE′ is the modified quadratic elongation. $10^5 \times (QE-1)$. where QE is the quadratic elongation defined by Robinson et al. (1971)
[b] φ in the notation of Born and Zemann (1964)
[c] Euler and Bruce (1965)
[d] after Armbruster et al. (1992)
[e] predicted from Novak and Gibbs 1971)
[f] after Armbruster and Geiger (1993)

bond lengths was observed by Armbruster et al. (1992) in pyrope-almandine solid solutions. Relatively constant Z−O bond lengths of 1.64±0.01 Å were also observed in all garnets analysed by Novak and Gibbs (1971). The small decrease in the Z-O bond length across the andradite-skiagite join is probably a response to the large decrease in the volume of the neighboring dodecahedral sites which acts to distort the tetrahedral sites.

The octahedral and tetrahedral O−O distances are sensitive to both cation substitutions on the particular site itself and on neighboring sites. Variations in the O−O distances depend on whether they are shared or unshared edges and, therefore, provide information about the structural distortion of the sites which is discussed in detail below (Table 4).

Structural Distortions

A number of different parameters exist for describing the degree of distortion or rotation of the octahedral and tetrahedral sites, but there is not standard measure for the dodecahedral site. The $\bar{3}$ point symmetry for the octahedral cation requires that all Y−O bond lengths are equal and that there are only 2 distinct O−Y−O bond angles. This limits the types of distortion to an expansion or contraction along the $\bar{3}$ axis, leading to an elongated or flattened octahedron. The distortion type serves as a structural discriminant for Winchell's (1933) classification scheme with the pyralspite and ugrandite garnet series having elongate and flattened octahedra respectively. The angle variance, AV, and quadratic elongation, QE, (Robinson et al. 1971) increase with increasing skiagite content in the almandine-skiagite garnets, indicating that substitution of Fe^{3+} for Al causes not only site inflation, but also a small amount of distortion (Table 5). Site distortion is also evident in the σ index (Euler and Bruce 1965), which is the angle between the $\bar{3}$ axis and the Y−O bond, and $\sigma = 54.736°$ for a regular octahedron. All almandine-skiagite garnets have $\sigma < 54.736°$, with a small decrease with increasing skiagite content, indicating an elongated octahedral site (Table 5).

Andradite has a flattened octahedral site and, therefore, $\sigma > 54.736°$ (Novak and Gibbs 1971). However, σ decreases with substitution of the skiagite component and a perfect octahedral site is reached in compositions of about 35 mol % skiagite (Table 5). This is also indicated by an AV of zero and QE = 1.0. Compositions richer in skiagite have octahedral sites elongated parallel to the $\bar{3}$ axis. A consequence of this change in figure is that the shared edges of the octahedra are longer than the unshared edges in andradite-rich compositions, but are shorter than the unshared edges in skiagite-rich compositions. Comparison with the almandine-skiagite garnets reveals that changes in the degree of distortion are greater when cation substitutions occur on neighboring sites rather than on the octahedral site itself. This is consistent with the fact that the neighboring dodecahedra share 6 out of 12 edges and can, therefore, exert a strong influence on the figure of the octahedral site.

The tetrahedral site is elongated parallel to the $\bar{4}$ symmetry axis. The tetrahedral sites are much more distorted than the octahedral sites (compare AV and QE for the 2 sites in Table 5). Changes in AV (or QE) are much less in almandine-skiagite garnets than in the andradite-skiagite solid solutions. This is expected since octahedra and tetrahedra only share apices so cation substitution on the octahedral site would have a minimal effect on distortion of the tetrahedral site. The least distorted tetrahedra occur in andradite, in agreement with the observation of Novak and Gibbs (1971) that the tetrahedra become more regular as the average ionic radius of the dodecahedral cation increases.

In addition to distortion, there is also a rotation of the tetrahedral sites. Born and Zemann (1964) define a rotational parameter, α, which measures the rotation of the site about the $\bar{4}$ symmetry axis and is defined as the angle between the crystallographic a-axis and the polyhedral edge shared between the tetrahedra and dodecahedra. As shown in Fig. 4, α increases almost linearly with increasing skiagite content in both solid solution series. The same trend occurs in the y oxygen positional parameter, suggesting that rotation of the tetrahedral site is accommodated by displacement of the oxygen atoms parallel to the b-axis (Table 2). An inverse relationship between α and the average ionic radius of the dodecahedral cation was observed by Born and Zemann (1964) and Meagher (1975) and more recently by Armbruster et al. (1992). They noted that structural constraints require the tetrahedral sites to rotate to higher angles of α as the size of the dodecahedral sites decreases. This is consistent with the trend observed in our andradite-skiagite garnets (Fig. 4). However, because there is no change in dodecahedral site occupancy across the almandine-skiagite join, a different mechanism involving the octahedral site must have a similar effect on the orientation of the tetrahedra. In the garnet structure, tetrahedra share each corner with neighboring octahedra, forming a continuous linkage. As the octahedral site enlarges with increasing skiagite content by substitution of Fe^{3+} for Al, the unit cell not only expands, but the linked tetrahedra rotate to higher angles of α in attempt to accommodate the larger octahedral site into the network.

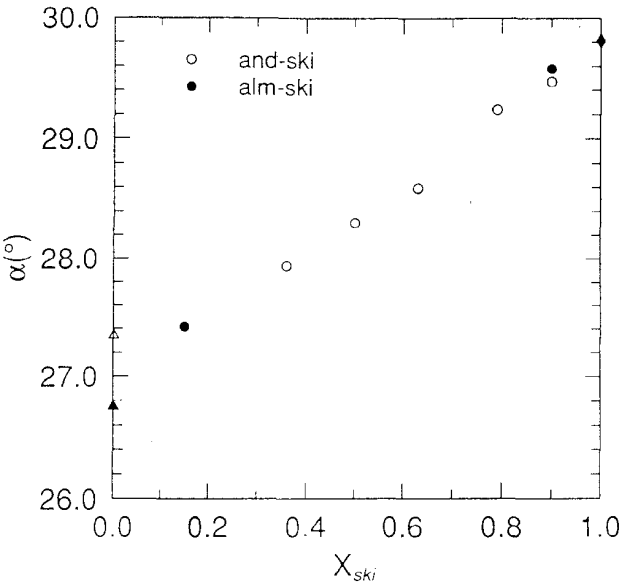

Fig. 4. The tetrahedral rotation parameter, α, (Born and Zemann 1965) plotted as a function of composition for almandine-skiagite and andradite-skiagite solid solutions. Data for the almandine (*closed triangle*) and andradite (*open triangle*) endmembers are from Armbruster et al. (1992) and Armbruster and Geiger (1993). The value for skiagite (*closed diamond*) was predicted by Novak and Gibbs (1971)

The parameter φ, defined by Euler and Bruce (1965), describes the rotation of the octahedral site about the $\bar{3}$ symmetry axis. φ was shown by Novak and Gibbs (1971) to be highly correlated with dodecahedral bond-angle strain, and therefore, provides an indirect measure of dodecahedral site distortion. In the limit of $\varphi = 0$, the $(X-O)_1$ and $(X-O)_2$ bond lengths become equal and the dodecahedron is bounded by 2 rectangular faces (Euler and Bruce 1965). There is an inverse relation between φ and increasing skiagite content in both solid solutions (Fig. 5, Table 5). The change in φ is more extensive across the almandine-skiagite join compared with the andradite-skiagite garnets and appears to be linear (Fig. 5). This contrasts with the arcuate trend observed along the andradite-skiagite join. The maximum degree of dodecahedral distortion appears to coincide with the garnet that has the least amount of octahedral distortion. Since φ and σ are both independent of the unit cell parameter, the nonlinearity cannot be related to excess volumes of mixing (see above).

A plot of φ versus σ provides a useful reference for discussing the relative effects of dodecahedral and octahedral substitutions on the garnet structure (Fig. 5). To provide a more generalised picture, we have combined our results along with literature data from Novak and Gibbs (1971) and Armbruster et al. (1992). As might be expected, it is the occupancy of the neighboring dodecahedral sites that has the greatest effect on octahedral distortion and vice versa. This is attributable to the fact that the octahedra and dodecahedra share some, but not all edges with each other so that inflation or deflation of one site causes a non-uniform response in the adjacent polyhedron. For example, there is a substantial change

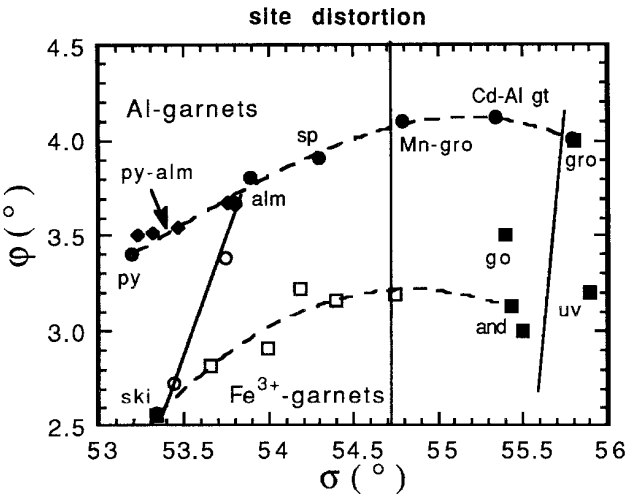

Fig. 5. Octahedral distortion parameter, σ, plotted against the dodecahedral distortion parameter, φ, (after Euler and Bruce 1964) for the two garnet solid solutions in this study (*open symbols*), Al-bearing and Ca-bearing garnets (*closed squares*) from Novak and Gibbs (1971), and pyrope-almandine solid solutions (*closed diamonds*) from Armbruster et al. (1992). The skiagite data are predicted values. The *vertical line* at $\sigma = 54.736°$ denotes an undistorted octahedral site. The octahedra are flattened and elongated in the $\bar{3}$ direction on the right and left sides of this line respectively

in dodecahedral site distortion (as measured by φ) with the substitution of Fe^{3+} for Al on the octahedral sites in almandine-skiagite solid solutions (Fig. 5). The same trend is apparent in the ugrandite garnets: grossular, goldmanite, uvarovite, and andradite. This suggests a common mechanism, independent of whether the dodecahedral site is occupied by a relatively large (Ca) or small (Fe^{2+}) cation. The smaller the octahedral cation, the more distorted the dodecahedral sites become. Dodecahedral site substitutions have a large effect on the octahedral site distortion with the same arcuate trend observable in the Al-garnet series as in our andradite-skiagite solid solutions (Fig. 5). A significant change in dodecahedral distortion also occurs due to substitution on the dodecahedral site itself. For example, the change in φ across the andradite-skiagite join is about 50% of that observed in the almandine-skiagite garnets. The maximum amount of dodecahedral distortion seems to occur in those garnets that have the most regular octahedral sites.

Cation Displacements

Calculated displacement ellipsoids reveal small magnitude, near isotropic motions for the octahedral (Al or Fe^{3+}) and tetrahedral (Si) cations in all garnets. In addition, the refined atomic displacement coefficients are consistent with rigid body motion of the ZO_4 groups

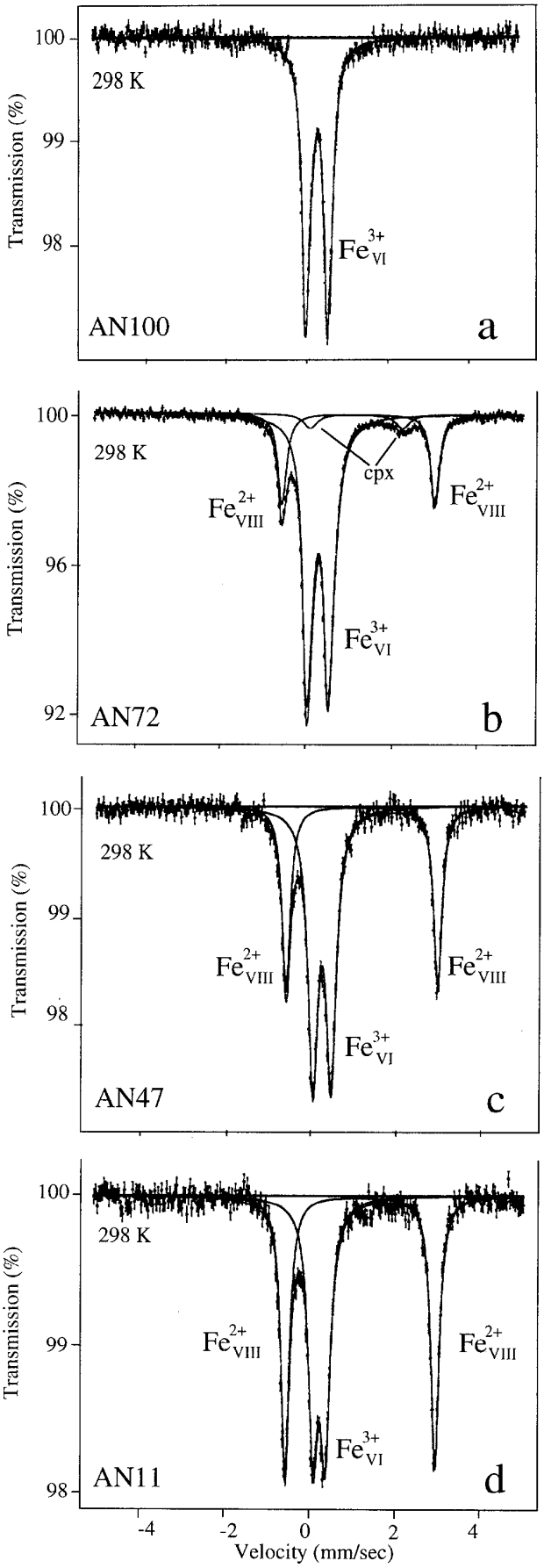

Fig. 6. Room temperature Mössbauer spectra of **a** and100, **b** and72, **c** and47, and **d** and11 garnet solid solutions. Site and valence assignments of the doublets are shown

and individual Y–O bonds. The rigid nature of these two sites was also reported by Gibbs and Smith (1965), Geiger et al. (1992) and Armbruster and Geiger (1993) for pyrope, almandine, and andradite respectively. In contrast, the dodecahedral cations show considerable anisotropic displacement. The ratio of the minor to major semiaxes for the 70% probability ellipsoids ranges from 0.6 to 0.7 for both solid solutions. The ratio of the intermediate to major semiaxes ranges from 0.8 to 0.95, indicating that the displacement ellipsoids are flattened. There is no significant variation with composition and the ranges are consistent with results for the almandine and andradite endmembers (Geiger et al. 1992; Armbruster and Geiger 1993). The major, intermediate and minor semiaxes of the displacement ellipsoids are in the $\langle 011 \rangle$, $\langle 01\bar{1} \rangle$ and $\langle 100 \rangle$ directions respectively. This orientation can be understood by considering the structural relationships between the different sites in the garnet structure. In the $\langle 011 \rangle$ and $\langle 01\bar{1} \rangle$ directions, there are channels in the network of octahedra and tetrahedra that are occupied by the dodecahedra. These are also the directions toward the longest unshared edges of the dodecahedra. As a result, the nearest cations in these directions are much further away compared with other orientations, and therefore, more freedom of movement would be permitted. For example, there is an alternation of dodecahedra and tetrahedra parallel to $\langle 100 \rangle$, which coincides with the minor semiaxis of the ellipsoid, or the direction of smallest displacement. Thus, anisotropy in the displacement of the dodecahedral cation is governed by structural constraints related to the positions of the neighboring sites.

Mössbauer Spectroscopy

Mössbauer spectra from both garnet solid solutions are simple. The spectra are composed of two well defined

Table 6. Mössbauer hyperfine parameters from room temperature and 80 K spectra of almandine-skiagite solid solutions

Sample	Comp X_{alm}	Thickness mg/cm^2 Fe	Fe^{2+}		FWHM mm/sec	Fe^{3+}		FWHM mm/sec	χ^2	$Fe^{3+}/\Sigma Fe$ area ratio Möss.	$Fe^{3+}/\Sigma Fe$ probe
			CS[a]	QS[a]		CS[a]	QS[a]				
Room temperature spectra											
alm1	1.00	4.23	1.31	3.54	0.25				3.06	trace	
alm6	1.00	3.45	1.31	3.53	0.26				2.08	trace	
aw18	0.98	1.41	1.29	3.51	0.25	0.27	0.23	0.38	1.52	0.059	0.013
aw14	0.97	1.50	1.30	3.52	0.26	0.31	0.13	0.39[b]	1.19	0.029	0.020
aw45	0.93	2.67	1.30	3.54	0.24	0.34	0.18	0.34	1.42	0.072	0.045
aw25	0.92	2.20	1.29	3.52	0.25	0.37	0.20	0.32	1.41	0.077	0.051
aw26	0.92	2.78	1.30	3.54	0.27	0.34	0.21	0.32	1.54	0.061	0.051
aw30	0.91	2.76	1.30	3.53	0.25	0.35	0.22	0.30	1.13	0.077	0.057
aw37a	0.85	3.17	1.30	3.54	0.24	0.33	0.23	0.25	1.05	0.136	0.091
aw37b	0.79	3.11	1.30	3.51	0.25	0.35	0.22	0.26	1.17	0.158	0.123
aw47	0.70	3.63	1.30	3.50	0.24	0.34	0.23	0.26	1.50	0.207	0.167
u458	0.71	3.08	1.29	3.51	0.28	0.35	0.23	0.28	2.04	0.191	0.162
u758	0.61	2.52	1.31	3.55	0.27	0.35	0.24	0.24	1.01	0.251	0.206
u541	0.59	3.13	1.30	3.52	0.25	0.34	0.25	0.28	1.34	0.271	0.215
u627	0.50	4.27	1.30	3.48	0.29	0.35	0.24	0.30	1.25	0.299	0.250
u765	0.48	3.68	1.30	3.49	0.23	0.35	0.24	0.25	1.17	0.297	0.257
u497	0.21	2.16	1.29	3.47	0.23	0.35	0.25	0.24	1.26	0.404	0.345
u524	0.18	4.94	1.31	3.50	0.23	0.35	0.24	0.26	2.43	0.404	0.353
u598	0.10	3.68	1.30	3.50	0.24	0.36	0.24	0.25	1.24	0.429	0.375
u636	0.01	2.50	1.31	3.46	0.23	0.35	0.24	0.26	2.11	0.459	0.398
u702	0.00	2.90	1.31	3.46	0.23	0.36	0.24	0.25	1.88	0.462	0.400
80 K spectra											
alm6	1.00		1.44	3.69	0.27	0.39	0.29	0.32	1.33	0.023	
aw14	0.97		1.44	3.70	0.28	0.34	0.40	0.48[b]	1.93	0.033	
aw45	0.93		1.42	3.65	0.33	0.39	0.11	0.41[b]	0.98	0.058	
aw25	0.92		1.41	3.64	0.32	0.41	0.20	0.31	1.05	0.058	
aw37a	0.85		1.42	3.64	0.29	0.42	0.20	0.28	1.25	0.112	
aw37b	0.79		1.44	3.70	0.25	0.43	0.20	0.30	1.08	0.137	
u458	0.71		1.42	3.63	0.29	0.42	0.19	0.32	0.96	0.177	
u627	0.50		1.44	3.70	0.25	0.46	0.24	0.28	1.51	0.289	
u497	0.21		1.45	3.67	0.24	0.46	0.23	0.25	1.30	0.378	
u598	0.10		1.45	3.68	0.24	0.47	0.23	0.26	1.23	0.402	
u636	0.01		1.45	3.65	0.24	0.46	0.23	0.28	1.50	0.443	

[a] mm/sec measured relative to α-Fe metal at 298 K. Uncertainties are about ±0.01 mm/sec for both QS and CS and ±0.01 for $Fe^{3+}/\Sigma Fe$. The area ratio assumes the same recoil-free fraction for Fe^{2+} and Fe^{3+} on the different sites

[b] constrained parameter

Table 7. Mössbauer hyperfine parameters from room temperature and 80 K spectra of andradite-skiagite solid solutions

Sample	Comp X_{and}	Thickness mg/cm^2 Fe	Fe^{2+}		FWHM mm/sec	Fe^{3+}		FWHM mm/sec	χ^2	$Fe^{3+}/\Sigma Fe$ area ratio Möss.	$Fe^{3+}/\Sigma Fe$ probe
			CS[a]	QS[a]		CS[a]	QS[a]				
Room temperature spectra											
aw63	1.00	1.47				0.40	0.55	0.25	0.99	1.000	1.000
aw39a	0.94	1.81	1.29	3.60	0.19	0.40	0.55	0.27	1.39	0.961	0.917
aw54a	0.93	1.61	1.30	3.59	0.23	0.39	0.55	0.26	1.34	0.937	0.905
aw39b	0.82	2.49	1.29	3.59	0.24	0.40	0.53	0.27	1.34	0.842	0.787
aw52a	0.72	4.67	1.29	3.56	0.24	0.39	0.50	0.29	1.41	0.781	0.704
aw52c	0.66	2.86	1.30	3.55	0.24	0.38	0.48	0.28	1.32	0.754	0.662
aw47	0.64	2.04	1.29	3.53	0.26	0.38	0.47	0.28	0.98	0.715	0.649
u769	0.60	2.71	1.29	3.53	0.31	0.37	0.47	0.28	1.32	0.732	0.625
u751a	0.47	2.02	1.30	3.55	0.24	0.37	0.43	0.28	0.99	0.637	0.557
u697	0.45	2.19	1.30	3.55	0.25	0.38	0.43	0.29	2.30	0.627	0.548
u654a	0.37	3.28	1.30	3.53	0.24	0.37	0.40	0.28	1.19	0.603	0.514
u684b	0.36	2.75	1.29	3.50	0.30	0.37	0.38	0.33	1.07	0.590	0.510
u751b	0.36	3.53	1.31	3.54	0.24	0.38	0.39	0.28	0.82	0.596	0.510
u714a	0.26	2.59	1.31	3.52	0.23	0.36	0.34	0.30	1.40	0.570	0.474
u610	0.22	2.89	1.30	3.51	0.24	0.36	0.34	0.29	1.36	0.537	0.461
u666	0.21	3.56	1.30	3.48	0.29	0.36	0.32	0.33	0.92	0.530	0.458
u739	0.11	3.85	1.31	3.49	0.26	0.35	0.29	0.28	0.99	0.502	0.428
u755	0.11	2.63	1.31	3.51	0.24	0.36	0.28	0.28	1.03	0.499	0.428
80 K spectra											
aw39a	0.94		1.41	3.65	0.29	0.48	0.54	0.26	1.31	0.924	
aw52a	0.72		1.42	3.65	0.28	0.48	0.49	0.31	1.22	0.723	
aw47	0.64		1.42	3.64	0.30	0.47	0.46	0.34	1.15	0.689	
u697	0.45		1.43	3.65	0.25	0.48	0.41	0.29	1.42	0.585	
u654a	0.37		1.43	3.65	0.25	0.46	0.39	0.29	1.56	0.555	
u666	0.21		1.43	3.64	0.24	0.46	0.32	0.27	0.91	0.484	
u755	0.11		1.43	3.63	0.32	0.45	0.27	0.36	1.04	0.471	
u739	0.11		1.44	3.64	0.28	0.44	0.26	0.30	1.06	0.457	

[a] mm/sec measured relative to α-Fe metal at 298 K. Uncertainties are about ±0.01 mm/sec for both QS and CS and ±0.01 for $Fe^{3+}/\Sigma Fe$. The area ratio assumes the same recoil-free fraction for Fe^{2+} und Fe^{3+} on the different sites

doublets with relative intensities that depend on composition (Figs. 6a–d and see Woodland and O'Neill 1993). The two doublets indicate the presence of Fe^{2+} and Fe^{3+}, each occupying a particular site. The Mössbauer spectra confirm that all garnets analysed in this study lie on either the almandine-skiagite or andradite-skiagite binary. There is no evidence of electron hopping between sites, at least at time scales $>10^{-7}$ seconds, nor is there magnetic splitting at least down to 80 K. The hyperfine parameters derived by fitting the Mössbauer spectra provide information about the oxidation state, coordination, and electronic environment of the Fe atoms in the garnet structure. The hyperfine parameters obtained at room temperature and 80 K from the almandine-skiagite and andradite-skiagite garnets are given in Tables 6 and 7 respectively.

Hyperfine Parameters and the Chemical Environment of Fe^{2+}

The dominant doublet in the almandine-skiagite garnets has a large center shift (CS) of 1.30 mm/sec at room temperature and 1.43 mm/sec at 80 K. The quadrupole splitting (QS) is also large, ≈3.5 mm/sec at room temperature and ≈3.7 mm/sec at 80 K. These values are characteristic of dodecahedrally coordinated Fe^{2+} (Amthauer et al. 1976). No statistically significant asymmetry is apparent between the low and high velocity peaks as is often reported for natural garnets (e.g. Luth et al. 1990; Amthauer et al. 1976). When two unconstrained peaks are fit, the χ^2 generally does not improve significantly and the difference between the resulting peak widths is within the uncertainty of ±0.01–0.02 mm/sec. The full width at half maximum (FWHM) for dodecahedral Fe^{2+} in both solid solutions is 0.19–0.35 mm/sec at both room temperature and 80 K, with most being between 0.22 and 0.26 mm/sec (Tables 6, 7). The narrow peak widths argue against $Ca-Fe^{2+}$ ordering in the andradite-skiagite garnets. If ordering did occur, a certain number of cation arrangements would be present, producing multiple Fe^{2+} doublets. Since the hyperfine parameters of each doublet would be only slightly different from each other, the result would be a single broadened doublet that was the summation of these doublets.

The dodecahedral Fe^{2+} CS remains the same at constant temperature in both solid solutions. The difference of 0.1 mm/sec between the room temperature and 80 K CS can be attributed to the temperature dependent second order Doppler shift. The QS at room temperature

shows a decrease of 0.1 mm/sec with increasing skiagite content in both solid solutions, attaining a minimum value of 3.46 mm/sec for skiagite (Tables 6 and 7). This behaviour is not apparent at 80 K, however. The constant values of CS and QS indicate the local electric charge density about the Fe atom remains unchanged in both solid solution series.

Hyperfine Parameters and the Chemical Environment of Fe^{3+}

The other doublet in the spectra has a much smaller CS and QS and grows in relative intensity with increasing skiagite or andradite content and can therefore be assigned to Fe^{3+} (Figs. 6a–d). The coordination of Fe^{3+} can be deduced by comparison with the ranges in hyperfine parameters for octahedral and tetrahedral Fe^{3+} in a variety of oxides and silicates, including garnets (Burns and Solberg 1990; Amthauer et al. 1976). The room temperature CS and QS of our garnets are 0.32–0.40 mm/sec and ≈0.21–0.55 mm/sec, respectively (Tables 6 and 7). These values indicate that the Fe^{3+} is in octahedral coordination. The FWHM of the Fe^{3+} doublet is slightly greater than for the Fe^{2+} doublet, ranging mostly between 0.25 mm/sec and 0.36 mm/sec at both room temperature and 80 K (Tables 6 and 7). The hyperfine parameters are not well constrained at almandine-rich compositions due to the poor resolution and low intensity of the Fe^{3+} doublet.

Contrary to that observed for dodecahedral Fe^{2+}, the hyperfine parameters corresponding to octahedral Fe^{3+} vary with composition. The variations are more subtle in the almandine-skiagite solid solutions than across the andradite-skiagite join. The CS increases by 0.02–0.03 mm/sec going from almandine-rich compositions to skiagite and it increases a further 0.04–0.05 mm/sec going from skiagite to andradite (Tables 6 and 7). These changes are quite small, although they do exceed the estimated overall uncertainty of ±0.01 mm/sec.

The ferric iron quadrupole splittings have very different trends in the two solid solutions. A small increase of about 0.03 mm/sec (at room temperature) occurs with increasing skiagite content along the almandine-skiagite join (Fig. 7, Table 6). It is difficult to quantify the actual magnitude of change due to the poor resolution of the Fe^{3+} doublet in almandine-rich (<7 mol% skiagite) compositions. The same small variation can be observed in the 80 K data set (Table 6). A much larger change of 0.30 mm/sec occurs across the andradite-skiagite binary at both room temperature and 80 K and is visually evident when the Fe^{3+} doublets in the Figs. 6b, 6c and 6d are compared (Table 7). Values of room temperature QS increase from 0.24 mm/sec in skiagite to 0.55 mm/sec in andradite (Fig. 7, Table 7). The QS values (and CS) obtained from pure andradite are in excellent agreement with those previously published (Amthauer et al. 1976; Schwartz et al. 1980; Geiger et al. 1990).

An explanation for the two distinctive QS trends in the almandine-skiagite and andradite-skiagite solid solutions is not readily apparent and cannot be uniquely

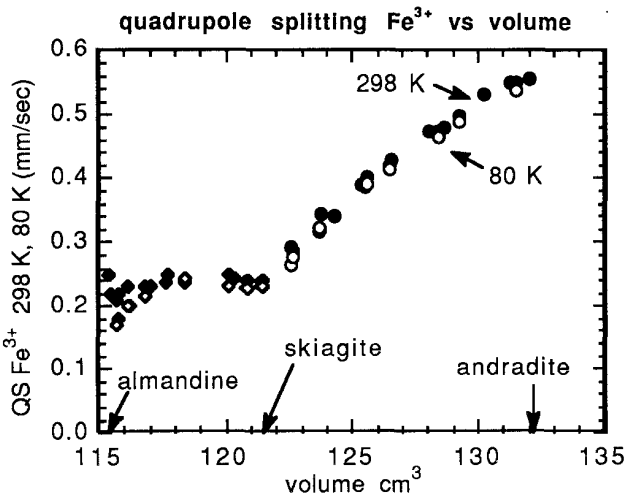

Fig. 7. Quadrupole splitting, QS, of the Fe^{3+} doublet at 298 K and 80 K plotted as a function of unit cell volume. Note the different behaviour of the almandine-skiagite and andradite-skiagite solid solutions

proved. A quadrupole split doublet arises when the interaction between the electric quadrupole moment and an electric field gradient (EFG) produces a non-cubic charge distribution about the Fe nucleus. There are two contributions to the EFG: an internal, or valence term, and an external, or lattice term (Parish 1986). Valence contributions originate from the non-bonding electron and bonding electron distributions. In high spin Fe^{3+}, each orbital contains 1 electron resulting in a spherically symmetric configuration. Thus, there are no non-bonding electrons to contribute to the EFG and the symmetry of the bonding electrons means that their contributions should cancel each other, yielding an overall valence contribution of zero (Dowty and Lindsley 1973; Parish 1986). The fact that the room temperature and 80 K QS are nearly the same supports a zero valence contribution since this term is much more sensitive to temperature than the lattice term (Dowty and Lindsley 1973).

The lattice term has 3 primary contributions (Amthauer et al. 1976):

1) A change in volume caused by simple inflation or deflation of a site,

2) distortions from cubic symmetry of the oxygen polyhedra,

3) next-nearest neighbor interactions.

Single-crystal data indicate that the progressive increase in volume from almandine to skiagite to andradite does not result only from simple inflation of the octahedral site (see above). Amthauer et al. (1976) reported a positive correlation between octahedral Fe^{3+} QS and molar volume in their set of 15 natural garnets. However, we find that this correlation applies only for volume changes due to dodecahedral site substitutions (andradite-skiagite) and not when octahedral site substitutions (almandine-skiagite) are responsible (Fig. 7).

Deviations from perfect cubic symmetry are expected to cause a non-zero QS in the Mössbauer spectrum. Considering that the lattice term is the only contribution

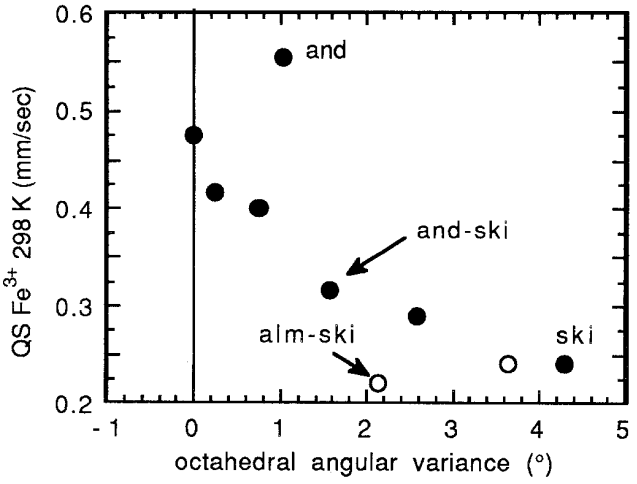

Fig. 8. Angular variance of the octahedral site plotted against the room temperature Fe^{3+} QS. Andradite-skiagite solid solutions pass through a minimum in angular variance, indicating an undistorted octahedral site at a composition of about 35 mol% skiagite. Angular variance for the andradite endmember was calculated from the data of Armbruster and Geiger (1993). The value for skiagite is predicted from Novak and Gibbs (1971)

to the EFG for high spin Fe^{3+}, the absolute value of QS should increase with increasing octahedral site distortion (Dowty and Lindsley 1973). Octahedral distortion, determined by X-ray diffraction, in the almandine-skiagite garnets is small and changes relatively little across the join (see above and Fig. 8). The virtually constant QS in these garnets is consistent with the observed small changes in distortion. In andradite-skiagite solid solutions, the octahedral site changes from oblate along the $\bar{3}$ axis in andradite to prolate in skiagite. The site is a perfect octahedron in compositions of about 35 mol% skiagite (Fig. 5). As a result, a minimum in QS would be expected in compositions near 35 mol% skiagite. However, this behaviour is not observed; the QS increases continuously across the join, seemingly independent of the degree of distortion (Fig. 8). The same behaviour was observed by Amthauer et al. (1976) for a Mn-bearing grossular which had a near perfect octahedral site, but had a relatively large QS (0.46 mm/sec at 77 K). It is apparent that the coordinating oxygen polyhedron is only partially responsible for the EFG experienced by the Fe^{3+} atoms and that there are other contributions which must come from greater distances.

The influence of next-nearest neighbors on octahedral Fe^{3+} QS was discounted by Amthauer et al. (1976) because the cation positions in the $Ia\bar{3}d$ space group are fixed. They proposed that the electronic charge distribution of the oxygen atoms was responsible for the observed trend in QS. However, this must also be a function of the next-nearest neighbor arrangement and their interactions with the oxygen atoms shared between the dodecahedral and octahedral sites. Since each octahedra shares edges with 6 dodecahedra, there are 7 possible arrangements of neighboring cations (i.e. 6Ca–0Fe, 5Ca–1Fe, etc.). The probability of each cation configuration in a given solid solution composition can be calculated assuming a random distribution of cations. Two to four different configurations are found to have probabilities above 0.15 in all compositions except those very close to each end-member. For example, for 36 mol% skiagite-64 mol% andradite, the following probabilities are obtained: 6Ca: 0.07, 5Ca–1Fe: 0.23, 4Ca–2Fe: 0.33, 3Ca–3Fe: 0.25, 2Ca–4Fe: 0.10, 1Ca–5Fe: 0.02, 6Fe: 0.002. Here, three configurations are highly probable, each creating a discrete environment that could contribute to the observed QS. This could arise from the large difference in the electronegativity of Ca and Fe^{2+} (1.0 vs 1.8), which would affect the character (ionicity) of the cation-oxygen bond, and in turn, alter the character of the bond with the neighboring Fe^{3+}. Changing the average bond character with next-nearest neighbor configuration and, therefore, with composition would have the effect of modifying the electronic charge distribution around the shared oxygen atoms, like that proposed by Amthauer et al. (1976). Several problems with this mechanism remain, however.

As one bond becomes more ionic, as is expected with increasing Ca content on the dodecahedral site, the neighboring bond with the octahedral cation (Fe^{3+}) should become more covalent in a compensatory fashion due to the "inductive effect" (e.g. Menil 1985). As the degree of covalency of the Fe^{3+}-O bond increases, the CS should decrease. However, the CS changes only slightly across the andradite-skiagite join and it increases with increasing Ca content which is the opposite to that expected (Table 7). The change in bond character should also lead to some positional disorder of the oxygen atoms. However, there is no evidence for this from the single-crystal refinements, where positional disorder would be reflected in increased atomic displacement factors (Table 3).

From a geometrical point of view, it is possible that the individual octahedral sites are distorted to different degrees than the value measured by X-ray diffraction which is averaged over about 10–20 unit cells or 20–40 octahedral sites. For garnets with compositions near 35 mol% skiagite, both oblate and prolate sites must be present in order to yield an average distortion-free octahedron. Such behaviour could result from different arrangements of next-nearest neighbors in the dodecahedral sites. However, this would lead to positional disorder and increased atomic displacement factors, which is not observed (Table 3).

Different arrangements of next-nearest neighbors, creating different chemical environments about the octahedral site, should lead to line broadening. This has been observed in natural Fe-bearing grossular-rich garnets, where the FWHM exceeded 0.5 mm/sec (Manning and Tricker 1977). The broadening was attributed to the substitution of Si by OH groups on some tetrahedral sites. Our garnets all have relatively narrow Fe^{3+} line widths which argues against more than one discrete chemical environment about the octahedral site.

Alternatively, the neighboring dodecahedral cations could be making a contribution to the EFG experienced by the octahedral Fe^{3+} atoms. In the garnet structure, the sites surrounding the octahedra always have a non-

cubic symmetry. The structural unit of dodecahedra and tetrahedra surrounding an octahedral site is a distorted trigonal antiprism and the environment about the Fe^{3+} atom never has perfect cubic symmetry. Changes in the dodecahedral site occupancy with composition would influence the EFG, leading to a change in the Fe^{3+} QS. Substitutions on the octahedral sites would have little effect since the octahedra are isolated from each other and, neighboring octahedral sites are too distant for any significant interactions to occur. This is consistent with the observed trends in Fe^{3+} hyperfine parameters in the two garnet solid solutions and would seem to explain the apparent disagreement between the octahedral site distortion observed by X-ray diffraction and the Fe^{3+} QS. However, as described above, the manner by which the substitution of Ca for Fe^{2+} effects the EFG, such as through a change in the bond character, remains elusive.

Area Ratios, Site Occupancy, and $Fe^{3+}/\Sigma Fe$

Relative peak areas of the Mössbauer spectra can, in principle, be used to determine the site occupancy of Fe^{2+} and Fe^{3+} and therefore, the $Fe^{3+}/\Sigma Fe$ ratio of the garnet. The relationship between the measured areas and the actual $Fe^{3+}/\Sigma Fe$ is complicated by thickness effects and different recoil-free fractions for the two Fe species on the two sites (e.g. Rancourt 1989). The simple composition of our garnets permits independent determination of $Fe^{3+}/\Sigma Fe$ using the electron microprobe and assuming perfect stoichiometry and charge balance to calculate the structural formulae. The Al and Ca contents give the mole fractions of almandine and andradite respectively in the two solid solution series. With a compositional uncertainty of ± 0.01–0.02 mole percent in the microprobe determinations, this yields an uncertainty in $Fe^{3+}/\Sigma Fe$ of about ± 0.01, which is similar to the estimated uncertainty in the Mössbauer method.

The measured area ratios at room temperature and 80 K are given in Tables 6 and 7, along with the $Fe^{3+}/\Sigma Fe$ ratios determined from the microprobe analyses. It is evident that the Mössbauer area ratios systematically overestimate Fe^{3+} contents in both solid solution series. The room temperature area ratios overestimate the actual $Fe^{3+}/\Sigma Fe$ ratios (from microprobe analysis) by 10–20% relative, while the area ratios from the 80 K spectra are higher by 5–10% relative (Fig. 9, Tables 6, 7).

The change in area ratio with temperature indicates that the overestimate of Fe^{3+} can be partly attributed to different recoil-free fractions for Fe in dodecahedral and octahedral coordination (Amthauer et al. 1976). To evaluate the relative difference in recoil-free fraction for two sites, i and j, the ratio, r, relating the line areas (A) or recoil-free fractions (f) at different temperatures, T_1 and T_2, can be defined as (Amthauer et al. 1976):

$$r_{i,j}^{T_2,T_1} = \frac{A_i^{T_2}/A_i^{T_1}}{A_j^{T_2}/A_j^{T_1}} = \frac{f_i^{T_2}/f_i^{T_1}}{f_j^{T_2}/f_j^{T_1}} \quad (1)$$

Amthauer et al. (1976) used the areas obtained from 4.5 K spectra as a reference since they could not independently determine the true $Fe^{3+}/\Sigma Fe$ content in their natural samples. Substituting the $Fe^{3+}/\Sigma Fe$ determined by microprobe for our garnet solid solutions as the reference, we obtain average values of r of 0.72 (6) at room temperature ($n=34$) and 0.87 (3) at 80 K ($n=17$). These values are apparently independent of composition and agree with those reported by Amthauer et al. (1976) for Fe-bearing pyrope and grossular; 0.76 (5) at 295 K and 0.92 (5) at 77 K. The relationship between the actual and expected $Fe^{3+}/\Sigma Fe$, derived using our value of r and Eq. (1), is shown in Fig. 9 at room temperature and 80 K. Comparison with the individual data points illustrates the consistency across the compositional range.

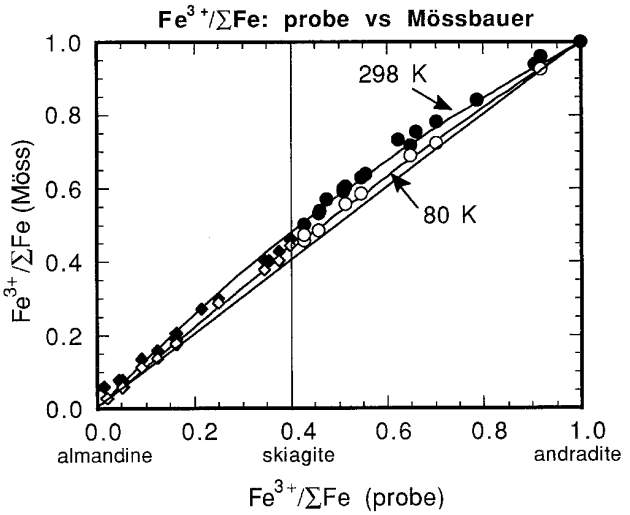

Fig. 9. Area ratios ($Fe^{3+}/\Sigma Fe$) derived from the room temperature and 80 K Mössbauer spectra plotted against the $Fe^{3+}/\Sigma Fe$ ratio determined by the microprobe. The andradite-skiagite garnets and almandine-skiagite solid solutions, together, encompass the entire range of $Fe^{3+}/\Sigma Fe$ from 0.0 to 1.0. The Mössbauer area ratios systematically over estimate the Fe^{3+} content, indicative of different recoil-free fractions for octahedrally and dodecahedrally coordinated Fe. The *lines* show the expected overestimate in Fe^{3+} at 298 K and 80 K derived from our values of "r", accounting for the difference in recoil-free fractions (see text)

A more accurate $Fe^{3+}/\Sigma Fe$ ratio may be obtained by extrapolating the measured area ratios to 0 K, where the relative difference in recoil-free fractions for the two sites is minimised. At low temperatues, f is closely approximated by:

$$f(T) = \frac{-E_r}{k\Theta_D}\left(\frac{3}{2} + \frac{\pi^2 T^2}{\Theta_D^2}\right) \quad (2)$$

where E_r is the recoil energy (1.95623×10^{-3} ev), k is Boltzmann's constant, and Θ_D is the characteristic Debye temperature. Substituting $\Theta_D = 340$ K and 400 K for dodecahedral and octahedral Fe respectively (Lyubutin et al. 1970; Lyubutin and Dodokin 1971) into Eq. (2), the 80 K area ratios can be extrapolated to 0 K using Eq. (1). The adjusted $Fe^{3+}/\Sigma Fe$ ratios are reduced systematically by a factor of 0.986, which improves the agreement with the values determined by the microprobe. A small overestimate in Fe^{3+} persists after this correction however, due to the differences in Θ_D for the

two sites. Instead of applying such a correction, it is recommended that peak areas be adjusted using Eq. (1) with $r=0.87$ or 0.72 for 80 K or room temperature data, respectively, in order to obtain the most accurate $Fe^{3+}/\Sigma Fe$ ratios. Since the correction to the area ratios is proportionately smaller at 80 K compared with room temperature, the ratios measured at 80 K will yield more consistent results. It should be noted that other effects such as sample thickness (Rancourt 1989) may influence the calculated area ratios, and therefore, must be carefully considered in sample preparation and data analysis. The nature of the correction for finite sample thickness is such that it reduces the measured $Fe^{3+}/\Sigma Fe$ ratio when ratios are <0.5 and increases the ratios when they are >0.5. The correction is zero when the $Fe^{3+}/\Sigma Fe$ ratio $=0.5$ (i.e. when the Fe^{2+} and Fe^{3+} doublets have the same areas). Following the method of Rancourt (1989), the most extreme correction to the $Fe^{3+}/\Sigma Fe$ ratio in our samples is ≈ 0.03 for intermediate compositions in both solid solution series. Note that while the thickness correction improves the agreement between the measured and actual $Fe^{3+}/\Sigma Fe$ ratios in the almandine-skiagite samples, it increases the discrepancy in the andradite-skiagite samples. Application to spectra of natural garnets should also be done with caution, since asymmetric dodecahedral Fe^{2+} doublets are often reported and the consequent influence on the measured area ratios is presently unknown.

Acknowledgements. This project was made possible in part by a fellowship to ABW from the Alexander von Humboldt Stiftung. Their support is gratefully acknowledged. Mark Brearley is thanked for his help in synthesising an andradite sample. R. Angel, N. Brown, W. Dollase, C. McCammon, and F. Seifert are thanked for their help and stimulating discussions during the course of the project. The manuscript benifited from the reviews of W. Dollase, C. McCammon and two anonymous reviewers.

References

Allen FM, Buseck PR (1988) XRD, FTIR, and TEM studies of optically anisotropic grossular garnets. Am Mineral 73:568–584

Amthauer G, Annersten H, Hafner SS (1976) The Mössbauer spectrum of ^{57}Fe in silicate garnets. Z Kristallogr 143:14–55

Armbruster T, Geiger CA (1993) Andradite crystal chemistry, dynamic X-site disorder, and structural strain in silicate garnets. Eur J Mineral 5:59–71

Armbruster T, Geiger CA, Lager GA (1992) Single crystal X-ray structure study of synthetic pyrope almandine garnets at 100 and 298 K. Am Mineral 77:512–521

Born L, Zemann J (1964) Abstandsberechnung und gitterenergetische Berechnungen an Granaten. Beitr Mineral und Petrogr 10:2–23

Burns RG, Solberg TC (1990) ^{57}Fe-bearing oxide, silicate, and aluminosilicate minerals. In: Coyne LM, McKeever SWS, Blake DF (eds) Spectroscopic Characterization of Minerals and their Surfaces pp 262–283. ACS Symposium Series 415, Am Chem Soc

Cressey G, Schmid R, Wood BJ (1978) Thermodynamic properties of almandine-grossular garnet solid solutions. Contrib Mineral Petrol 67:397–404

Dowty E, Lindsley DH (1973) Mössbauer spectra of synthetic hedenburgite-ferrosilite pyroxenes. Am Mineral 58:850–868

Engi M, Wersin P (1987) Derivation and application of a solution model for calcic garnet. Schweiz Mineral Petrol Mitt 67:53–73

Euler F, Bruce JA (1965) Oxygen coordinates of compounds with garnet structure. Acta Crystallogr 19:971–978

Ganguly J, Cheng W, O'Neill HStC (1993) Syntheses, volume, and structural changes of garnets in the pyrope-grossular join: implications for stability and mixing properties. Am Mineral 78:583–593

Geiger CA, Newton RC, Kleppa OJ (1987) Enthalpy of mixing of synthetic almandine-grossular and almandine-pyrope garnets from high temperature solution calorimetry. Geochim Cosmochim Acta 51:1755–1763

Geiger CA, Lottermoser W, Amthauer G (1990) A temperature dependent ^{57}Fe Mössbauer study of synthetic almandine-grossular and almandine-pyrope garnets: A comparison. Terra Abstr 2:75

Geiger CA, Armbruster T, Lager GA, Jiang K, Lottermoser W, Amthauer G (1992) A combined temperature dependent ^{57}Fe Mössbauer and single crystal X-ray diffraction study of synthetic almandine: Evidence for the Gol'danskii-Karyagin effect. Phys Chem Minerals 19:121–126

Geller S (1967) Crystal chemistry of the garnets. Z Kristallogr 125:1–47

Gibbs GV, Smith JV (1965) Refinement of the crystal structure of synthetic pyrope. Am Mineral 50:2023–2039

Hackler RT, Wood BJ (1989) Experimental determination of Fe–Mg exchange between garnet and olivine and estimation of Fe–Mg mixing properties in garnet. Am Mineral 74:994–999

Holdaway MJ (1972) Thermal stability of Al–Fe epidote as a function of fO_2 and Fe content. Contrib Mineral Petrol 37:307–340

Huckenholz HG, Yoder HS (1971) Andradite stability relations in the $CaSiO_3-Fe_2O_3$ join up to 30 Kb. N Jb Mineral Abh 114:246–280

Huckenholz HG, Lindhuber W, Springer J (1974) The join $CaSiO_3-Al_2O_3-Fe_2O_3$ of the $CaO-Al_2O_3-Fe_2O_3-SiO_2$ quaternary system and its bearing on the formation of granditic garnets and fassaitic pyroxenes. N Jb Mineral Abh 121:160–207

Huckenholz HG, Lindhuber W, Fehr KT (1981) Stability relationships of grossular + quartz + wollastonite + anorthite. I The effect of andradite and albite. N Jb Mineral Abh 142:223–247

Huckenholtz HG, Fehr KT (1982) Stability relationships of grossular + quartz + wollastonite + anorthite. II The effect of grandite-hydrograndite solid solution. N Jb Mineral Abh 145:1–33

Kingma KJ, Downs JW (1989) Crystal structure analysis of a birefringent andradite. Am Mineral 74:1307–1316

Koziol AM (1990) Activity-composition relationships of binary Ca–Fe and Ca–Mn garnets determined by reversed, displaced equilibrium experiments. Am Mineral 75:319–327

Kress VC, Carmichael ISE (1988) Stoichiometry of the iron oxidation reaction in silicate melts. Am Mineral 73:1267–1274

Liou JG (1973) Synthesis and stability relations of epidote $Ca_2Al_2FeSi_3O_{12}(OH)$. J Petrol 14:381–413

Luth RW, Virgo D, Boyd FR, Wood BJ (1990) Ferric iron in mantle-derived garnets, implications for thermobarometry and for the oxidation state of the mantle. Contrib Mineral Petrol 104:56–72

Lyubutin IS, Dodokin AP (1971) Temperature dependence of the Mössbauer effect for Fe^{2+} in dodecahedral coordination in garnet. Sov Phys Crystallogr 15:1091–1092

Lyubutin IS, Dodokin AP, Belyaev LM (1970) Temperature dependence of the Mössbauer effect for octahedral iron atoms in garnet. Sov Phys Solid State 12:1100–1101

Manning PG, Tricker MJ (1977) A Mössbauer spectral study of ferrous and ferric ion distributions in grossular crystals: Evidence for local crystal disorder. Can Mineral 15:81–86

Meagher EP (1975) The crystal structures of pyrope and grossularite at elevated temperatures. Am Mineral 60:218–228

Menil F (1985) Systematic trends of the ^{57}Fe Mössbauer isomer shifts in (FeO_n) and (FeF_n) polyhedra. Evidence of a new correlation between the isomer shift and the inductive effect of the competing bond $T-X(->Fe)$ (where X is O or F and T any

element with a formal positive charge). J Phys Chem Solid 46:763–789
Novak GA, Gibbs GV (1971) The crystal chemistry of the silicate garnets. Am Mineral 56:791–825
O'Neill HStC, Wood BJ (1979) An experimental study of Fe–Mg partitioning between garnet and olivine and its calibration as a geothermometer. Contrib Mineral Petrol 70:59–70
Parish RV (1986) Mössbauer spectroscopy and the chemical bond. In: Dickson DP, Berry FJ (eds) Mössbauer Spectroscopy pp 17–69. Cambridge University Press, Cambridge U.K.
Perchuk LL, Aranovich LY (1979) Thermodynamics of minerals of variable composition: Andradite-grossular and pistacite-clinozoisite solid solutions. Phys Chem Minerals 5:1–14
Rancourt DG (1989) Accurate site populations from Mössbauer spectroscopy. Nuclear Instruments and Methods in Physics Research B44:199–210
Robinson K, Gibbs GV, Ribbe PH (1972) Quadratic elongation: A quantitative measure of distortion in coordination polyhedra. Science 172:567–570
Roth RS, Dennis JR, McMurdie HF (1987) Phase Diagrams for Ceramists, volume VI, American Ceramic Society, Westerville, Ohio, USA
Schwartz KB, Nolet DA, Burns RG (1980) Mössbauer spectroscopy and crystal chemistry of natural Fe–Ti garnets. Am Mineral 65:142–153
Shannon RD (1976) Revised effective ionic radii and systematic studies of interatomic distances in halides and chalcogenides. Acta Cryst A32:751–767
Soós M, Jánosi M, Dódony I, Lovas G (1991) Anomalous grandite garnet from Recsk, Mátra Mts. (N-Hungary) Part I. Chemical composition, optical and diffraction properties. N Jb Mineral Mh 1991:76–86
Takeuchi Y, Haga N, Umisu S, Sato G (1982) The derivative structure of silicate garnets in grandite. Z Kristallogr 158:53–99
Winchell AN (1933) Elements of Optical Mineralogy, Part II Description of Minerals. 3rd ed John Wiley and Sons Inc., New York, USA, 185
Woodland AB, O'Neill HStC (1993) Synthesis and stability of $Fe_3^{2+}Fe_2^{3+}Si_3O_{12}$ garnet and phase relations with $Fe_3^{2+}Al_2Si_3O_{12}-Fe_3^{2+}Fe_2^{3+}Si_3O_{12}$ solutions. Am Mineral 78:1000–1013
Woodland AB, Wood BJ (1989) Electrochemical measurement of the free energy of almandine ($Fe_3^{2+}Al_2Si_3O_{12}$) garnet. Geochim Cosmochim Acta 53:2277–2282